Design, Modeling, and Verification of a High-Pressure Liquid Dielectric Switch for Directed Energy Applications

Joshua J. Leckbee, *Member, IEEE*, Randy D. Curry, *Member, IEEE*, Kenneth F. McDonald, *Member, IEEE*, W. Ray Cravey, *Member, IEEE*, Glenn Anderson, and Susan Heidger

***Abstract*—A high-power liquid dielectric switch is being developed to satisfy the requirements for future directed energy applications. A flowing, high-pressure liquid dielectric was chosen for the design of a megavolt class switch operating at 100 pps. This paper reports on the design philosophy, modeling, and experimental results of a full size, single-shot prototype 250–300 kV concept validation test (CVT) switch which can transfer kilojoules per pulse. Analysis of design criteria and scaling for a compact, 100-pps, kilojoule, high-voltage switch are presented. Optimization studies indicate that a pressure range of 6.9–13.8 MPa (1000–2000 psi) appears to be ideally suited to a flowing dielectric rep-rate switch.**

***Index Terms*—Directed energy, high pressure, high-voltage switch, liquid dielectric, megawatt switch, oil switch, rep-rate switch, spark gap.**

I. Introduction

DIRECTED energy research has fueled the need for more compact switches for use in high repetition rate systems. A switch is required near term that will switch 250 kV–1 MV and currents on the-order of 50 kA–250 kA. Concurrently the switch must have a 50 ns or less risetime and be able to operate at up to 150 pps into a 4–5-Ω load. As shown in Table I, the switch must be able to transfer up to 0.5 coulombs/pulse and have an operational lifetime of 10^7–10^8 pulses.

The switch proposed by the University of Missouri-Columbia team is based on a flowing dielectric that is pressurized hydraulically. In 1992, subnanosecond risetime, kilohertz rep-rate oil switches were built and demonstrated that could operate up to 290 kV with a rep rate of 200 pps and at 170 kV at 1000 pps [1]. The demonstrated risetime into a 97-Ω resistive load was 280 ps. The modulator system, which utilized medium pressure oil switches, transferred 50 J/pulse [1]. Since that time repetitive oil switches that could operate at 100–1000 pps and transfer multikilojoule energies have remained elusive, and have not been demonstrated. Recent research in high-power liquid dielectric switching has focused on switches that transfer energies of less than 1 J/pulse [2], [3].

TABLE I
SWITCH REQUIREMENTS

Voltage	250-1000kV
Current	50-250kA
Risetime	<50ns
Charge Transfer	~0.5 Coulombs/pulse
Jitter	<<50ns
PRF	50-150pps
Pulse Width	50-500ns
Lifetime	10^7-10^8 pulses

An initial engineering analysis indicated that two issues, bubble size and bubble lifetime, or oscillation period, needed to be resolved if scaling of flowing dielectric oil switches for transfer of kilojoule pulses were to be realized near term. When a high-voltage pulse is applied to a flowing dielectric switch, and the switch breakdown voltage is reached, a streamer is launched and subsequent avalanche ionization and breakdown of the dielectric results [4]. The arc then ionizes the dielectric medium and a gas bubble is formed between the electrodes. At atmospheric pressure, the diameter of the bubble expands well beyond the electrode separation distance. Early calculations indicated that the growth and oscillation period of the gas bubble would limit operation of the flowing dielectric switch to well below the goal of 100–150 pps at transfer energies in excess of a kilojoule. Subsequent growth of the gas bubble and formation of microbubbles as the gas bubble collapsed would then prevent recovery of the oil switch if voltages were reapplied before the entire volume of oil in the switch could be exchanged. As an outgrowth of the early modeling, it was found that pressurization of the fluid was required to reduce the volume and concurrently the radius of the gas bubble. By minimizing the size and lifetime of the bubbles produced, the volume of oil that must be exchanged between shots is greatly reduced.

Modeling and design of the prototype switch includes the analysis of the formation of bubbles and carbon, the breakdown properties of the liquid, the ability to clear the electrode gap with flowing liquid, electric field stress, and mechanical stress. A single-shot test stand has been modified to facilitate the testing of a concept validation test (CVT) switch. The test stand produces 250-kV pulses into a 1.6-Ω load under single-shot operation. The modeling efforts, the design, and the test results ob-

Manuscript received September 29, 2003; revised July 24, 2004. This work was supported by the USAF, AFRL at Wright Patterson AFB, under Contract USAF F33615-01-C-2191.

J. J. Leckbee, R. D. Curry, and K. F. McDonald are with the Department of Electrical Engineering, University of Missouri–Columbia, Columbia, MO 65211 USA.

W. R. Cravey is with Alpha-Omega Power Technologies, Albuquerque, NM 87109 USA.

G. Anderson is with The Boeing Company, St. Louis, MO 63166 USA.

S. Heidger is with Air Force Research Laboratory, AFRL/PRPE, Wright Patterson Air Force Base, OH 45433 USA.

Digital Object Identifier 10.1109/TPS.2004.835955

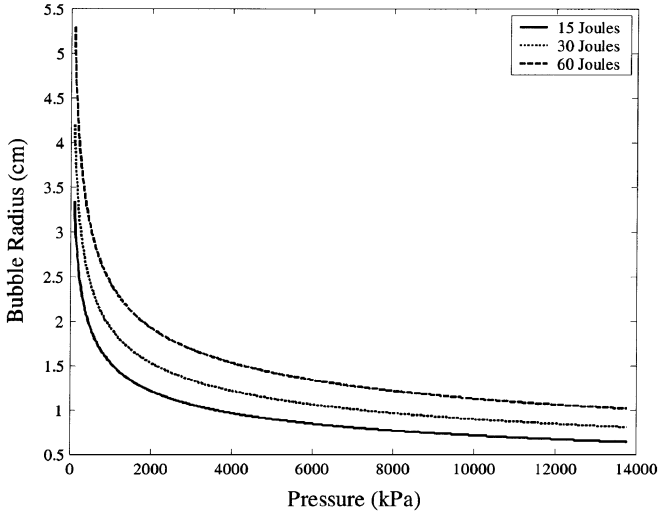

Fig. 1. Plots of the maximum bubble radius versus pressure for arc losses of 15–60 J.

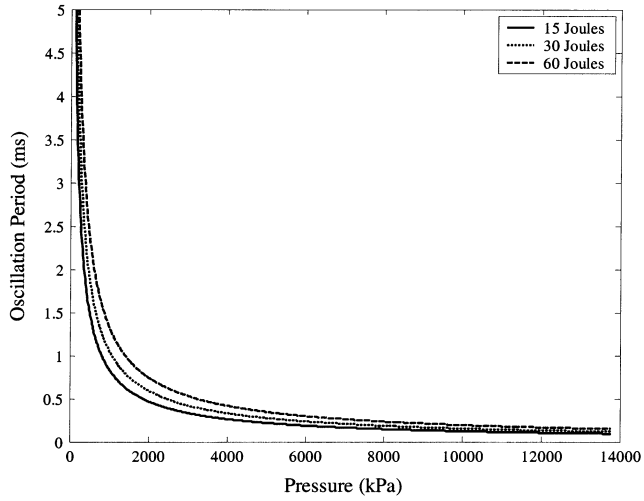

Fig. 2. Plots of the oscillation period versus pressure for arc losses of 15–60 J.

tained using the CVT switch will be described, along with the experimental observations from the switch tests.

II. Bubble Size and Oscillation

When an arc is formed in a liquid, chemical bonds are broken and byproducts are formed. In the case of oil, these byproducts include carbon particles and gases. Rayleigh developed equations to describe the characteristics of a bubble over time as it collapses [5]. The same equations derived to explain the collapse of a bubble have been applied to the unconstrained expansion of gas bubbles. From these equations the maximum size of the bubble and the time elapsed during one period, from formation to collapse, can be calculated. As (1) and Fig. 1 show, the maximum radius of the bubble formed increases with increasing energy lost in the arc and decreases with increasing hydraulic pressure. Equation (1) calculates the maximum bubble radius (meters) from the energy used to form the bubble (joules) and the hydraulic pressure of the liquid (pascals). As a first-order, worst-case approximation, it can be assumed that all of the energy dissipated in the arc is used to produce the bubble. In reality, not all of the energy dissipated in the arc is consumed by bubble formation [6]. Other sources of energy loss include the formation of shock waves, thermal and convective losses to the electrodes, and heating of the liquid [7], but models of these loss mechanisms for high-energy discharges in high-pressure liquids do not exist.

Bubbles formed due to charge injection into liquids using a point plane electrode geometry have been shown to behave as explained by Rayleigh [8], [9]. Electrical discharges in water under vacuum have also shown agreement with Rayleigh's equations, though it was found that only about 15% of the energy dissipated in the arc was used to produce bubbles [6]. Experiments with laser–produced bubbles showed that as little as 1% of the laser energy was converted into kinetic energy in the expanding bubble wall [10]. Experiments in electrical triggering of liquid spark gaps also showed that not all of the energy lost in the arc is transferred to the bubble wall as kinetic energy [7]. Experiments with underwater explosives have also shown a correlation with Rayleigh's equations [11].

Experiments with underwater explosions and arc-induced bubbles in unconstrained geometries have shown that after a bubble collapses it can rebound and go through a number of expansion and contraction cycles before going back into solution or breaking up into smaller bubbles (microbubbles) [6], [11]. The period of the damped oscillation of the bubble in an unconstrained environment, given in (2) and Fig. 2, also increases with increasing energy loss in the arc and decreases with increasing background pressure [9], [12]. The oscillation time (seconds) is calculated from the density (kg/m^3), energy (joules), and the pressure (pascals). Based on the experimental setup of the single-shot testing of the CVT switch, the arc drop losses and thus the energy growth of the gas bubble were bounded using the arc loss calculated by the J. C. Martin formulae. The bounded parameter space ranged from 15–60 J with 30 J being the average. When bubbles are formed in a constrained geometry, such as a small electrode gap as described below in the CVT switch, the bubbles are not allowed to expand isotropically and are more prone to jetting and breaking up due to instabilities rather than exhibiting a damped oscillation. The bubbles will expand as predicted by the oscillation theory and, thus, a calculation of the oscillation period provides an approximation of the time required for the bubble to form and then oscillate or breakup into smaller bubbles. The gases will remain in the switch for several oscillation periods regardless of whether they oscillate or breakup into smaller bubbles

$$r_{\max} = \left(\frac{3}{4\pi}\frac{E}{P}\right)^{1/3} \tag{1}$$

$$T_{\text{osc}} = 1.135\frac{\rho^{1/2}E^{1/3}}{P^{5/6}}. \tag{2}$$

III. Dielectric Liquids

The high-pressure dielectric switch has been tested using polyalphaolefin (PAO), a dielectric coolant fluid. The synthetic oil PAO poses somewhat reduced environmental concerns in case of leaks or spills, when compared with hydrocarbon oils.

TABLE II
OIL PROPERTY COMPARISON

Properties	Diala AX	PAO
Dielectric Constant	2.2-2.3	2.1
Breakdown Voltage		
ASTM D877 (tested in Lab)	36.4kV	39.7kV
ASTM D877 (manufacturer ratings)	>35kV	50kV

The electrical properties of the PAO are comparable to those of Shell Diala AX, a common transformer oil, see Table II. A comparison to Diala AX is presented since transformer oils are typically used in pulsed high-voltage experiments. The PAO used in the experiments was deaerated prior to the tests, but was not dewatered. The breakdown values are reported in accordance with the ASTM D877 voltage breakdown standard [13]. This standard utilized a small test cell with 2.54-cm diameter flat electrodes, separated by 0.245 cm. The voltage is a sinusoidal voltage that is ramped up at a rate of 3 kV/s until breakdown occurs. The test is then repeated at 1-min intervals and the mean value is reported as the breakdown strength of the liquid.

IV. BREAKDOWN VOLTAGE

The breakdown voltage of a dielectric depends on a number of factors. Some of the factors which effect breakdown strength are the charge time, the electrically stressed area of the electrodes, and the density of the dielectric. Work done by J. C. Martin relates the breakdown field strength (MV/cm) to the charge time (μs) and the stressed area (cm^2), defined as the area of the electrode stressed to 90% of the peak field [14]. Calculations using the J. C. Martin formulae show that breakdown field strength increases for shorter pulse times and smaller stressed areas. The relationship developed by Martin has been modified to estimate the negative polarity breakdown strength of oil (3), [15]. The values $\mathrm{E_{max}}$ and $\mathrm{E_{mean}}$ are the maximum electric field at the electrode surface and the average field between the gap. Using (3), the breakdown field strength can be calculated for the CVT switch as tested on the single-shot test stand. The switch had 3.8-cm diameter hemispherical electrodes and a 0.2-cm electrode spacing which results in an electrode stressed area of $1.2*10^{-5}$ m^2. Using this stressed area and a t_{eff} of 0.5 μs, the breakdown strength can be estimated at 1 MV/cm

$$E_{\mathrm{br}} = 1.41\left(\frac{.48}{t_{\mathrm{eff}}^{1/3}A^{0.075}}\right)\left[1+0.12\left(\frac{E_{\max}}{E_{\mathrm{mean}}}-1\right)^{1/2}\right]. \tag{3}$$

Previous work on the breakdown of liquid dielectrics under pressure shows that as pressure increases, the breakdown strength increases for small electrode areas [16]. The pressure dependence of breakdown strength has been used as evidence to support the theory that liquid breakdown is initiated by the formation and subsequent electrical breakdown of a gas bubble in the liquid [17]. Kao also reported that transformer oil pressurized up to about 2.4 MPa (350 psi) showed a gain in the breakdown strength of up to 35%–40%, over those at atmospheric pressure [9]. Based on this information and extrapolating out to high pressures, approximately a 35%–40% increase in the dielectric strength of oil at 10.3 MPa (1500 psi) is expected. Other experiments indicated that the pressure dependence of breakdown strength decreases for very fast rising pulses [18]. Since the pressures of interest are so much greater than those considered by Kao, this extrapolation should be considered as a very rough approximation. Experimental data collected using the CVT switch showed a gain of only 20%–25%, as shown in Fig. 9.

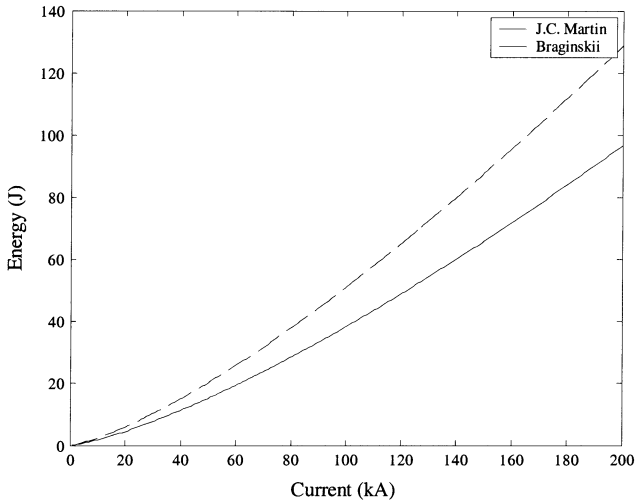

Fig. 3. Comparison of the J. C. Martin energy loss approximation to the Braginskii loss method for a range of currents.

V. SWITCH ENERGY LOSS

The energy dissipated in the arc must be calculated to determine the properties of the gas bubble formation. The switch loss can be obtained using J. C. Martin's equation for switch loss, (4). In this equation, the energy loss (joules) is calculated from the peak voltage (kV), the driving impedance (Ω) and the resistive risetime (μs). The equation for resistive risetime (5) can be used to calculate the exponential resistive phase transition time (ns), given the driving impedance and the breakdown field strength (MV/cm). The exponential resistive phase transition time describes the time period when the resistance of the arc channel decreases exponentially. Calculations of the CVT switch loss based on (4) and a charge voltage of 250 kV predict an energy loss of about 37 J. As shown in Figs. 1 and 2, the bubble radius is bounded as a function of the arc loss from 15–60 J. The energy loss calculation is approximate and has not yet been verified in the high-pressure regime of interest

$$E = \left(\frac{V^2}{4Z}\right)\tau_r \tag{4}$$

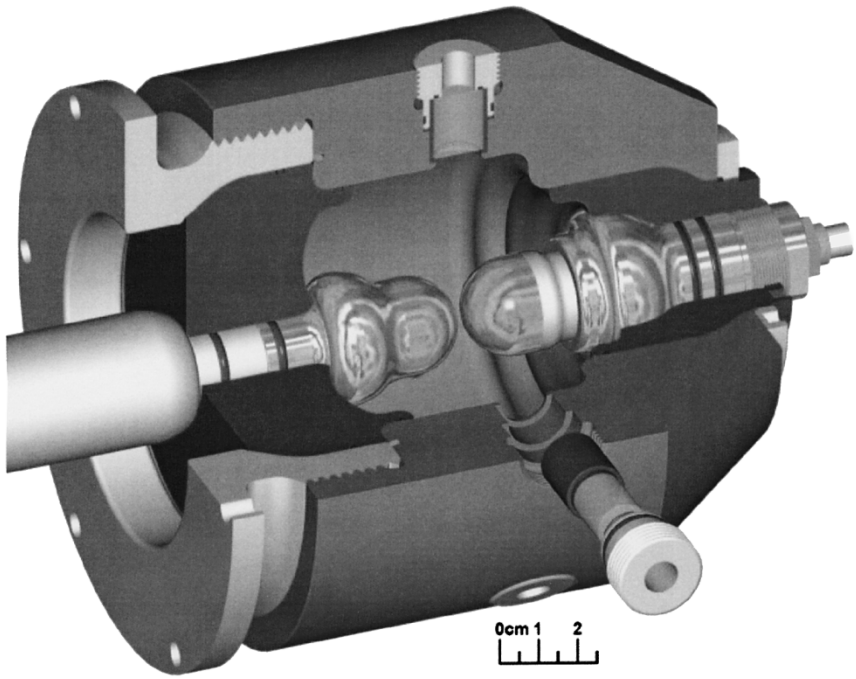

Fig. 4. Cross section of the CVT switch with hemispherical electrodes, view ports, and oil ports.

$$\tau_r = \frac{5}{Z^{1/3} E_{\rm br}^{4/3}}. \tag{5}$$

The change in voltage across a switch can be described using the equations for resistive risetime, inductive risetime, and total risetime. During the resistive risetime, the arc is formed and the resistance of the arc decreases rapidly from an open circuit to an impedance much less than the driving impedance. The inductive risetime describes the time while the arc is expanding, and the inductance is decreasing. The total risetime, shown in (7), gives the time for the voltage across the switch to decrease from 90% to only 10% of the peak value. Based on these equations, the CVT switch with a charge voltage of 250 kV is expected to have a total (10%–90%) risetime of 10–11 ns when driven with an impedance of 1.6 Ω

$$\tau_L = \frac{L}{Z} \tag{6}$$

$$\tau_{\rm total} = 2.2\tau_r + 2.2\tau_L. \tag{7}$$

The switch loss can also be calculated from the current through the switch and the time varying arc resistance obtained using Braginskii's formula, (8). The resistance is obtained using (8), which describes the time varying arc radius, and assumes a constant conductivity, as described by T. Martin [19], [20]. The equation for the time varying arc radius determines the radius of the arc (cm) from the density of the dielectric (g/cm^3), the current (kA), and the time (μs). Utilizing this method to calculate the energy loss in the switch requires only the current through the switch, the length of the electrode gap, and the conductivity of the arc. With Tom Martins assumption of a conductivity of 600 $(\Omega \cdot {\rm cm})^{-1}$, and the anticipated current though the CVT switch, the energy loss is about 30 J or 33% less than that estimated by Martin's formulae

$$r = 0.093 \rho^{-1/6} I^{1/3} t^{1/2}. \tag{8}$$

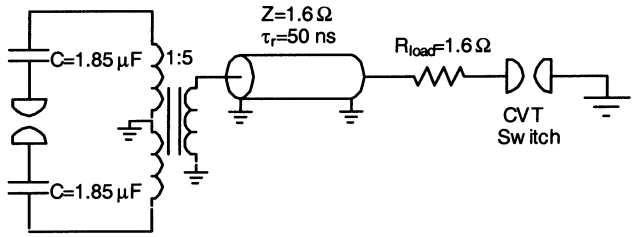

Fig. 5. Single-shot experimental test circuit for CVT switch.

Both methods of calculating the energy are intended as an approximation. A comparison of the two methods of energy calculation has been made with respect to current through the switch (see Fig. 3). The equation derived by Braginskii for an arc formed in air (8) was used for the comparison. A comparison to experimental data is necessary to determine which method is most accurate for a particular experimental setup. The experimental comparison of the two methods is beyond the scope of this program. However, it is interesting to note that the curves overlay within a few percent if the Braginskii equation is multiplied by 1.33.

VI. Experimental Program and CVT Switch Design

The switch shown in Fig. 4 was integrated into the single-shot test stand as shown in Fig. 5. The circuit consisted of two capacitors, each 1.85 μF, charged to opposite voltages and then switched into the primary of a 1:5 stepup transformer. The system pulse charges the 1.6-Ω water transmission line to 250–300 kV in 1–1.2 μs with a $t_{\rm eff}$ of 0.5 μs, producing a 100-ns pulse when discharged. A short oil transmission line was used to connect the larger water transmission line to the smaller diameter output switch. The load resistor consists of six liquid resistors whose parallel combination yields a resistance of 1.6 Ω and is embedded in the short oil section between the

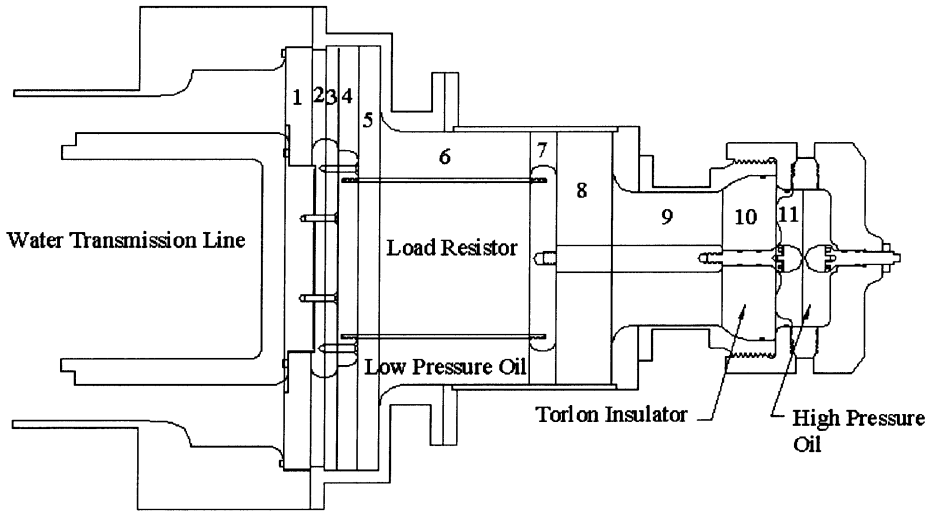

Fig. 6. This figure shows a cross section of the single-shot system. The system was divided into 11 section, which are numbered, and each was modeled as a discrete transmission line.

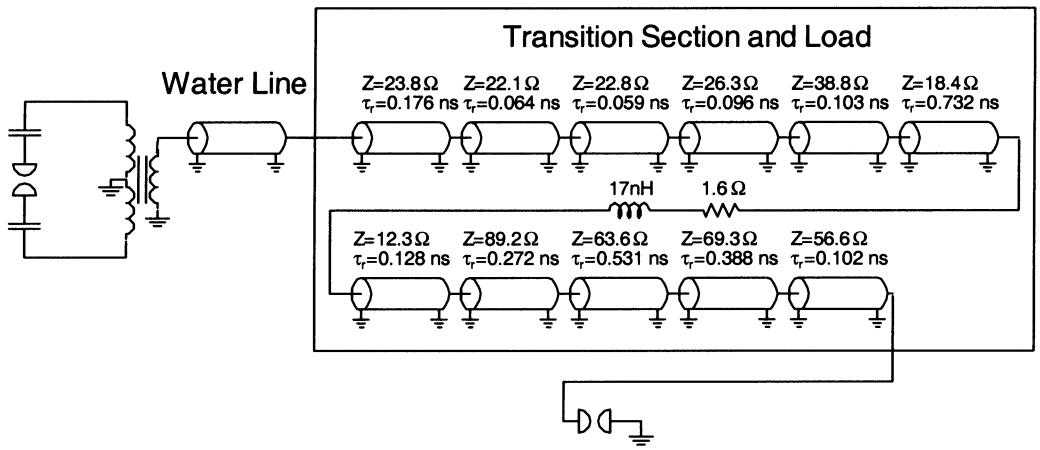

Fig. 7. Transmission line model used to simulate the risetime of the circuit.

water line and the output switch. The oil section and load resistor are shown in Fig. 5 as a resistor.

Three electrical diagnostics were used to monitor the voltage and current. A Rogowski coil was used to measure the current, and two integrated d-dot probes were used to measure voltage. One d-dot probe is located in the water transmission line, and the other was placed in the short oil section between the load resistor and the output switch. Both were calibrated with an external Tektronix 6015 probe and a Pearson current monitor.

Optical diagnostics were used to observe the formation of bubbles and other byproducts. Videos of the breakdown byproducts were captured using a Kodak Ektapro HG Model 2000 Imager using the maximum frame rate of 2000 frames per second with an exposure time of 983 μs. These images were used to view the formation and oscillation of bubbles and the formation and expansion of carbon clouds. A second camera, the DRS Hadland, Ltd. Imacon 200 camera was used to acquire high-speed images of the bubbles and the carbon clouds to determine the expansion velocity. The Imacon 200 is capable of capturing 12 images with a wide range of exposure times and spacing between exposures. The exposure time can range between 5 ns and 5 ms for each frame. Each camera was positioned to view the space between the electrodes through one of the 1.31-cm switch optical ports. Two different lighting schemes were used. Two high-intensity CW light sources were used to light the electrode gap for the Kodak video sequences. The light sources were aligned to the view ports at angles of 45° and 135° with respect to the camera. A Photogenics flashlamp was utilized to backlight the electrode gap for the high-speed Imacon 200 photos through an optical port at an angle of 135° with respect to the camera.

VII. Circuit Simulation

The CVT test circuit, as described above, was modeled using PSpice. The circuit was simulated using a discrete transmission line approximation of the 1.6-Ω water line, load resistor, transition section, and CVT switch. A cross section of the single-shot system is shown in Fig. 6. Due to the rapid transition changes in impedance in the oil section, the system was divided into 11 sections and each was modeled as a discrete transmission line. The transmission line model is shown in Fig. 7. Another circuit model was tested which represented the oil transition section as a discrete LC network. Both models gave excellent re-

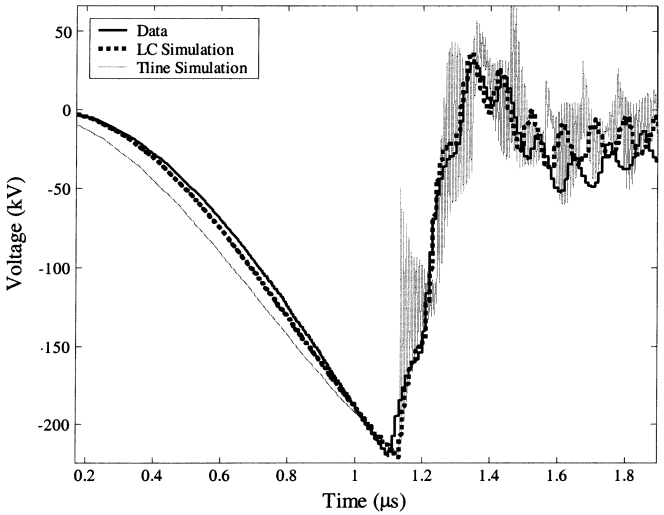

Fig. 8. Comparison of voltage data to circuit simulations. The voltage was measured using the d-dot probe mounted in the water pulse forming line.

sults. Both the discrete LC network model and the transmission line model are compared to experimental data in Fig. 8. The calculated risetime of the circuit was 100 ns with the switch transition section and the inductance of the load included. The predicted 10–11 ns risetime of the switch was used for the simulations. The observed output voltage of the circuit Fig. 8, as measured in the water transmission line, decays to zero in 100 ns when the switch closes since the pulse forming line is terminated with a matched load. The simulated voltage characteristics accurately match the d-dot probe signals. The voltage across the switch could not be accurately measured due to the relatively low-voltage drop across the switch.

VIII. Breakdown Versus Pressure

Experiments with the CVT switch have shown that pressurizing a dielectric increases its breakdown strength. Experiments were run using 3.81-cm diameter hemispherical electrodes and a gap spacing of 0.2 cm. The results of these experiments are plotted in Fig. 9. Each data point represents an average of ten pulses for a given pressure. The error bars represent one standard deviation for the set of data at that pressure and the curve fit is a second-order polynomial least-squares approximation. The data shows that the breakdown strength increases by about 25%–30% as the pressure increases from atmospheric pressure to 10.3 MPa (1500 psi). This is much less than the 40% gain expected from extrapolating Kao's data out to higher pressures [16]. The experiments reported by Kao, are for a very limited data set, nine pulses, up to pressure of only 2.4 MPa (350 psi). The discrepancy in gain predicted by extrapolating previous experiments and the results of the CVT test are due to the extremely different parameter spaces and error in extrapolating out to more than four times the highest pressure previously studied [16]. The apparent discrepancy can also be attributed in part to the time dependence of the pressure effects on breakdown strength [18]. The unconditioned electrodes had a statistical deviation of $\pm 10\%$, which decreased to $\pm 6.5\%$ after 45 conditioning shots.

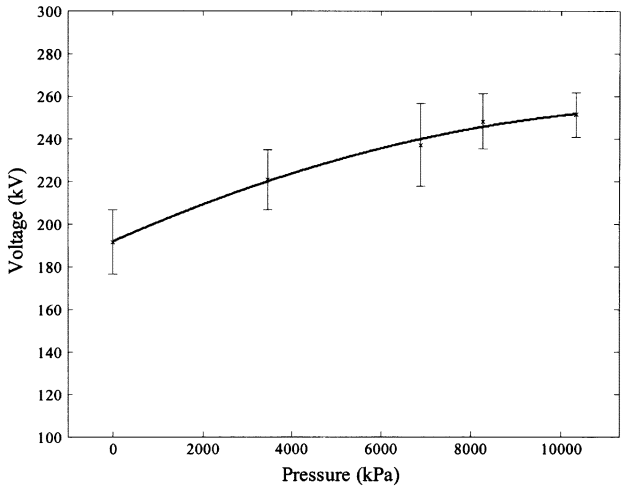

Fig. 9. This plot shows the average breakdown voltage of PAO for a 0.2-cm gap at various pressure with one standard deviation error bars.

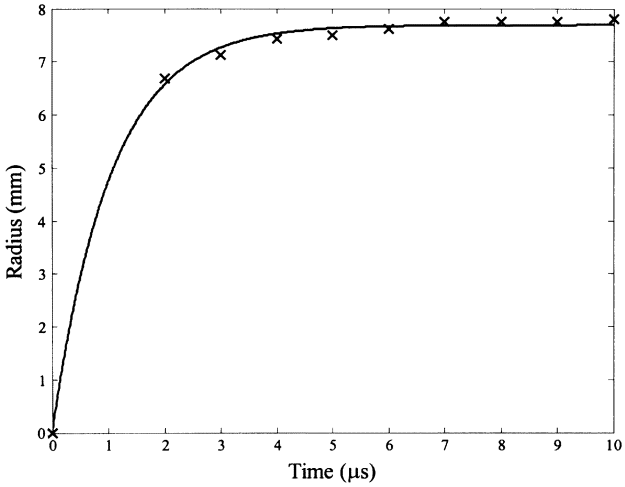

Fig. 10. This plot shows the radius of a carbon cloud formed at 13.8 MPa (2000 PSI) as a function of time.

IX. Breakdown Byproducts

The formation of bubbles and carbon was observed using the two camera systems previously described. The Kodak video camera was helpful in determining the expansion rate of the carbon clouds, Fig. 10, and the volume of gas and carbon that would need to be removed in rep-rate operation. The photographs of the bubbles and carbon relied on the reflection of light from the high-intensity light sources. This type of photography does not capture events such as shock waves, but it is very useful in that carbon clouds can easily be distinguished from gaseous bubbles. The carbon cloud is seen as a dark cloud expanding from the arc site. The interface of the gas and liquid at the bubble wall reflects light. This results in bubbles appearing as white spots, or as small white rings. Figs. 11 and 12 show bubbles and carbon formed at atmospheric pressure and at 13.8 MPa (2000 psi).

The maximum radius of the bubbles formed at atmospheric pressure could not be determined because of the limited field of view. The 1.31-cm optical port in the switch housing provided

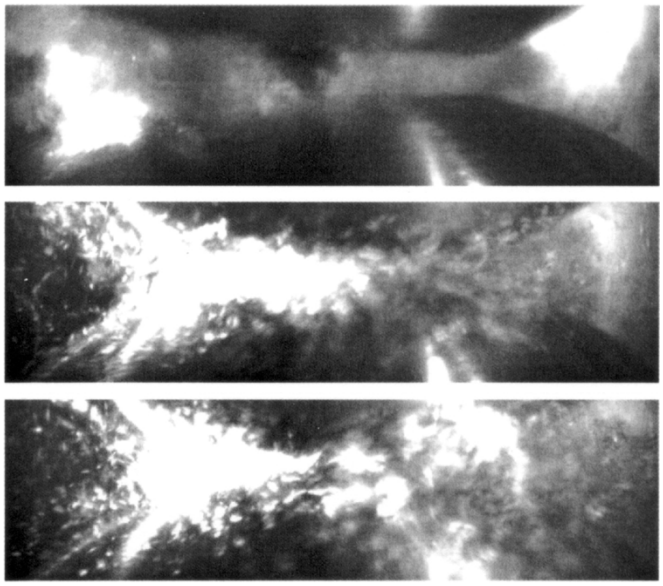

Fig. 11. Picture of bubbles formed by an arc at atmospheric pressure. The switch housing is lit from the front and from behind, with light seen reflecting off of the bubbles. The frames were taken 3, 8, and 13 ms after the arc formation.

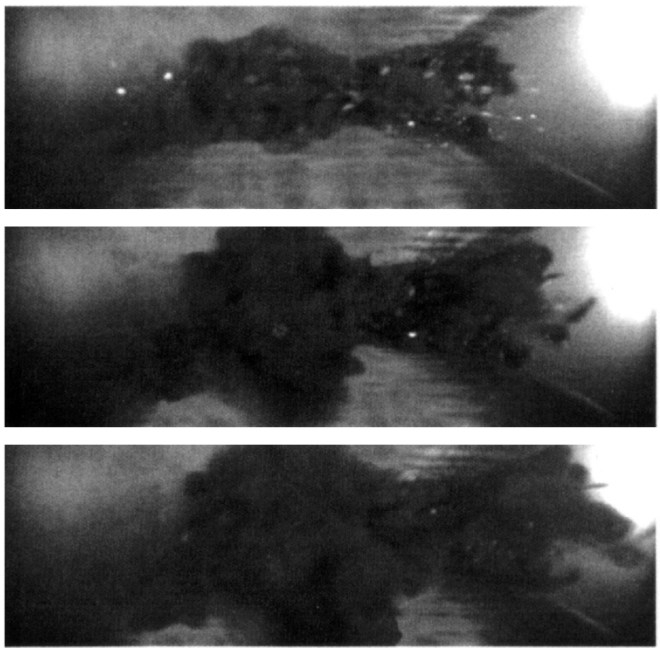

Fig. 12. Pictures of bubbles and carbon formed by an arc at 13.8 Mpa (2000 PSI). The carbon is seen as a dark cloud, while the bubbles reflect light and are seen as small white spots in the carbon cloud. Frame timing is the same as Fig. 11.

a field of view of about 2 cm in diameter. Theoretical calculations predict, that at atmospheric pressure, the maximum bubble radius would be about 4 cm and, thus, much too large to be seen in the photographs. Due to the geometric restriction of the electrodes, the bubbles are not allowed to expand isotropically, as a result, the bubbles break up into smaller bubbles instead of oscillating and form microbubbles. At atmospheric pressure, the window is too small to view the complete expansion of the bubble, or to view the bubble as it collapses. High-speed photos taken with the Imacon 200 found that the initial expansion velocity of the bubble was about 25 m/s.

For high pressures, above 3.4 MPa (500 psi), the bubbles were small enough that they did not extend out of the field of view; however, the carbon clouds were large enough to occlude the bubble and prevent accurate measurements of its size. Based on the size of the carbon clouds and the visible bubbles, it was determined that at these high pressures, the equations overestimate the size of the bubbles formed. At 6.9 MPa (1000 psi), a switch dissipating 15–60 J of energy would be expected to form bubbles with a diameter around 1.5–2.5 cm and an oscillation period of 0.2–0.3 ms. Photographs have shown that the bubbles are much smaller and also quickly break up into microbubbles, less than 1 mm in diameter, and some appear to be reabsorbed into solution after about 20 ms. The initial bubble formation was occluded by the carbon cloud expansion and was not resolved. At the higher pressures, the formation of a single bubble was not found. The equations used to predict bubble dynamics indicate that for an energy deposition of 15–60 J in oil at 10.3 MPa (1500 psi), bubbles of about 0.7–1.1-cm diameter should be produced. Photographs indicate that bubbles formed at and above this pressure are much smaller, and quickly break up into microbubbles (see Fig. 12). The fact that the bubbles formed in the oil are smaller than predicted by (1) agrees with the finding that only a fraction of the energy dissipated in an arc is used to produce gas bubbles [6].

As the hydraulic pressure increases, the formation of the carbon is more localized. At atmospheric pressure, some carbon is produced, but the amount is either small enough that it is not visible in photographs or the expanding bubble wall disperses the carbon out of the electrode gap. At 3.4 MPa (500 psi), enough carbon is produced to be visible as a cloud. At higher pressures, the carbon is seen in photographs as a dark cloud.

The expansion of the carbon cloud is much slower than that of the bubbles formed in the low-pressure regime. Measurements of the bubbles formed at atmospheric pressure showed initial expansion velocities of about 25 m/s. Expansion of the carbon cloud is very slow in comparison. Fig. 10 shows that while the initial radial expansion can be 3–5 m/s, the expansion slows to less than 0.125 m/s after about 2 ms. For a flowing oil switch, where the oil will sweep the byproducts out of the electrode gap, the slowly expanding carbon cloud lowers the flow required for recovery of the voltage holdoff.

Flowing oil experiments on the CVT switch with various electrode geometries have shown that the carbon and small bubbles can easily be cleared from the gap. The results from these experiments indicate that flow rates of about 0.5–1 l/s at pressures of 7–13 MPa will be required for 100–200-pps operation of a switch transferring kilojoules per pulse.

X. Summary

A single-shot CVT high-pressure dielectric switch has been designed, constructed, and tested. It was found that at high pressures the equations describing bubble formation overestimate the size of the bubbles formed. This, we believe, is due to the loss mechanisms not included in the first-order model. These

mechanisms include radiative, convective and collisional losses to the electrode surface and to the vapor/liquid interface. The losses also include acoustic and shock waves generated by the expansion of the gas bubble. It was also found that at high pressures, carbon formation was more localized and that bubble formation is eliminated or reduced by high-pressure operation. The breakdown strength of the PAO oil was found to increase with increasing pressure up to about 10.3 MPa (1500 psi). CVT experiments indicate that a switch operating in the 6.9–10.3 MPa (1000–1500 psi) range would minimize the flow requirements for rep-rate operation and that fabrication of high pressure, high-energy switches is well within today's state of the art.

REFERENCES

[1] R. Curry, P. Champney, C. Eichenberger, J. Fockler, D. Morton, R. Sears, I. Smith, and R. Conrad, "The development and testing of subnanosecond-rise, kilohertz oil switches for the generation of high-frequency impulses," *IEEE Trans. Plasma Sci.*, vol. 20, pp. 383–392, June 1992.

[2] S. Xiao, S. Katsuki, J. Kolb, S. Kono, M. Moselhy, and K. Schoenbach, "Recovery of water switches," in *Proc. 25th Power Modulator Symp.*, Hollywood, CA, 2002, pp. 471–474.

[3] S. Xiao, J. Kolb, S. Kono, S. Katsuki, R. Joshi, M. Laroussi, and K. Schoenbach, "High power, high recovery rate water switch," in *Proc. 14th Int. Pulsed Power Conf.*, Dallas, TX, 2003, pp. 649–652.

[4] E. Kuffel and W. S. Zaengl, *High Voltage Engineering*, Oxford: Pergammon, 1984.

[5] J. W. Strutt and A. Rayleigh, "On the pressure developed in a liquid during the collapse of a spherical cavity," in *Scientific Papers*. Cambridge, U.K.: Cambridge Univ. Press, 1920, vol. 6.

[6] G. L. Chahine, G. S. Frederick, C. J. Lambrecht, G. S. Harris, and H. U. Mair, "Spark-generated bubbles as laboratory-scale models of underwater explosions and their use for validation of simulation tools," in *Proc. Shock Vibrations Symp.*, vol. 2, Albuquerque, NM, Nov. 1995, pp. 265–276.

[7] P. K. Watson, W. G. Chadband, and W. Y. Mak, "Bubble growth following a localized electrical discharge and its relationship to the breakdown of triggered spark gaps in liquids," *IEEE Trans. Elect. Insulation*, vol. 20, pp. 275–280, Apr. 1985.

[8] R. Kattan, A. Denat, and N. Bonifaci, "Formation of vapor bubbles in nonpolar liquids initiated by current pulses," *IEEE Trans. Elect. Insulation*, vol. 26, pp. 656–662, June 1991.

[9] S. Oliveri, R. Kattan, and A. Denat, "Numerical study of single-vapor-bubble dynamics in insulating liquids initiated by electrical current pulses," *J. Appl. Phys.*, vol. 71, no. 1, pp. 108–112, Jan. 1992.

[10] A. Larsson, A. Sunesson, J. Garmer, and S. Kroll, "Laser-triggered electrical breakdown in liquid dielectrics," *IEEE Trans. Dielect. Elect. Insulation*, vol. 8, pp. 212–219, Apr. 2001.

[11] R. H. Cole, *Underwater Explosions*. Princeton, NJ: Princeton Univ. Press, 1945.

[12] H. F. Willis, "Underwater explosions," British Rep. WA-47-21, 1941.

[13] ASTM D877 Data Sheet [Online]. Available: http://www.astm.org

[14] J. C. Martin, "Nanosecond pulse techniques," *Proc. IEEE*, vol. 80, pp. 934–945, June 1992.

[15] R. J. Adler, "Pulse power formulary," North Star Research Corp., June 2002.

[16] K. C. Kao and J. B. Higham, "The effects of hydrostatic pressure, temperature, and voltage duration on the electric strength of hydrocarbon liquids," *J. Electrochem. Soc.*, vol. 108, pp. 522–528, 1961.

[17] A. Sharbaugh, J. Devins, and S. Razad, "Progress in the field of electric breakdown in dielectric liquids," *IEEE Trans. Elect. Insulation*, vol. 13, pp. 249–276, Apr. 1978.

[18] K. C. Kao and J. McMath, "Time-dependent pressure effect in liquid dielectrics," *IEEE Trans. Elect. Insulation*, vol. 5, pp. 64–68, Feb. 1970.

[19] S. I. Braginskii, "Theory of the development of a spark channel," *Soviet Phys. JETP*, vol. 7, no. 6, pp. 1068–1074, Dec. 1958.

[20] T. H. Martin, J. F. Seamen, and D. O. Jobe, "Energy losses in switches," in *Proc. IEEE 9th Int. Pulsed Power Conf.*, vol. 1, Albuquerque, NM, 1993, pp. 463–470.

Joshua J. Leckbee (M'03) received the B.S.E.E. and M.S.E.E. degrees from the University of Missouri–Columbia in 2002 and 2004, respectively. His thesis in on the design and testing of high-pressure liquid spark gap switches.

He was with Sandia National Laboratory, Albuquerque, NM, where he is engaged in the development of pulsed-power apparatus.

Randy D. Curry (S'79–M'82–S'82–M'84) received the M.S.E.E. degree from Texas Tech University, Lubbock, in 1985 and the Ph.D. degree in applied physics from St. Andrews University, St. Andrews, U.K., in 1992.

From 1984 to 1995, he worked in industry in the areas of plasma physics pulsed power and electron beam applications and environmental research. He has actively pursued the application of these technologies for the disinfection of microorganisms and the destruction of chemicals in water and food. In 1995, he joined the Department of Electrical Engineering faculty at the University of Missouri–Columbia. As a faculty member, he has investigated new applications of electron beams and high-power UV sterilization, including surface disinfection.

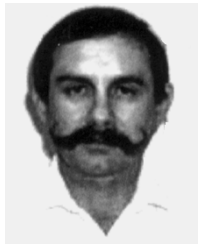

Kenneth F. McDonald (M'92) received the B.S.E.E. degree from Northern Arizona University, Flagstaff, the M.S.E.E. degree from Texas Tech University, Lubbock, and the Ph.D. degree in electrical engineering from the University of Missouri–Columbia.

He has conducted extensive research in the area of microbial decontamination and sterilization employing ultraviolet photon sources and chemical photosensitizers. While at Sandia National Laboratory, Albuquerque, NM, the Naval Research Laboratory, and several small high-tech companies, he worked in the areas of plasma physics, magnetic fusion, pulsed power, lasers, microwaves, and particle beams. He is currently a Research Professor at the University of Missouri–Columbia.

W. Ray Cravey (S'86–M'87–S'87–M'88) received the M.S.E.E. degree from Texas Tech University, Lubbock, in 1988.

He is the President and CEO of Alpha-Omega Power Technologies, Albuquerque, NM, which specializes in industrial pulsed-power systems. He has extensive experience in high-voltage pulsed power, high-speed diagnostics, measurements, signal analysis, and EM modeling. He has published over 14 papers in the area of pulsed power. He also has extensive experience in high-voltage, high-speed, liquid, and gas switching. In addition, he has spent several years in developing ultracompact solid-state switched modulators utilizing surface mount technology.

Glenn Anderson received the B.Eng. in applied science, the B.A. degree in environmental studies, and the M.S. degree in engineering mechanics from the State University of New York at Stony Brook.

He has 28 years of experience in aircraft design and development. He has spent his career developing air vehicle subsystems for various McDonnell Douglas air vehicles. He has also been Environmental Controls and Hydraulic Power System Functional Supervisor directing research in ECS, high-pressure hydraulics, and flight control actuation. He also has extensive experience in electrical power systems and was the Team Leader for electrical power and electric actuation for the JSF/integrated subsystem technology. He served as Technology Lead for Advanced Subsystems in the Air Vehicle Advanced Design Group in the Advanced Aircraft and Missiles Division, The Boeing Company, St. Louis, MO, and was Program Manager for the Electrical Power for Pulse Directed Energy for UAV, a research-order sponsored by AFRL-PR. His current assignment is with the Directed Energy Group in Advanced Combat Aircraft Systems. He served for ten years as Chairman of the Military Aircraft and Helicopter Panel in the Fluid Power, Control, and Actuation Committee (A6) of the Society of Automotive Engineers. He holds two U.S. patents: Environmental Controls and Fl.

Susan Heidger received the Ph.D. degree in physics from Case Western Reserve University, Cleveland, OH, in 1993.

She was a Research Associate for the National Research Council in the Surface Science Branch at the NASA-Lewis (now Glenn) Research Center. She joined the Propulsion Directorate (Power Division) of the Air Force Research Laboratory, Wright Patterson Air Force Base, OH, in 1998. Her current research efforts include high-power and high-temperature dielectrics and packaging, chemical vapor deposited diamond applications, high-power switches, and high-energy density capacitors.